ACS APPLIED POLYMER MATERIALS

pubs.acs.org/acsapm Article

# Poly(ethyleneimine)/Poly(acrylic acid) Multilayer Coatings with Peripherally Bound *Staphylococcus aureus* Bacteriophages Have Antibacterial Properties

Martin Müller,* Birgit Urban, Gopala Krishna Mannala, and Volker Alt

Cite This: *ACS Appl. Polym. Mater.* 2021, 3, 6230−6237 Read Online

ACCESS | Metrics & More | Article Recommendations | Supporting Information

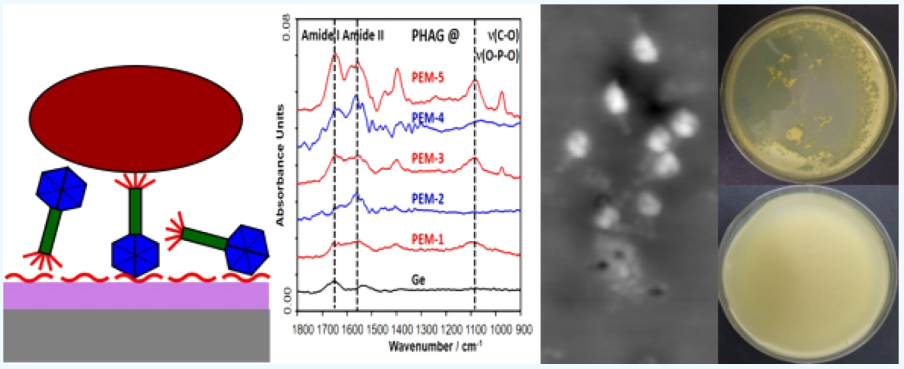


**ABSTRACT:** Herein, polyelectrolyte (PEL)-based coatings including peripherally bound bacteriophages (PHAG) at model substrates are reported to showcase their applicability on surgically relevant implants with respect to surface protection against bacterial proliferation and biofilm formation. The established layer-by-layer concept based on the consecutive adsorption of oppositely charged PEL was applied to generate polyelectrolyte multilayer (PEM) coatings with either a cationic or anionic excess surface charge. PHAG were bound at the outermost layer of such PEM coatings utilizing electrostatic interaction forces. Branched poly(ethyleneimine) (PEI) and poly(acrylic acid) (PAA) as cationic and anionic PEL, respectively, and the*Escherichia coli* T4 bacteriophage (T4 PHAG) and the *Staphylococcus aureus* bacteriophage (S.a. PHAG) were used. At first, PEM of PEI/PAA were consecutively adsorbed from solutions at germanium model substrates with $z = 4$ and 5 adsorption steps providing PAA-terminated PEM-4 and PEI-terminated PEM-5, which were characterized by surface-sensitive in situ attenuated total reflection Fourier transform infrared spectroscopy. Second, both T4 and S.a. PHAG were bound to these PEM showing a higher bound amount at cationic PEM-5 compared to anionic PEM-4. Electrostatic interaction forces between anionic capsid proteins and respective PEM are suggested. Furthermore, scanning force microscopy revealed typical overall size (200−250 nm) and shape (head/tail) features of the bound PHAG and supported qualitatively the preference for cationic PEM-5 by number. Finally, PEM-4 and PEM-5 were deposited at standard agar plates, S.a. PHAG were bound to those PEM, and plaque assay was performed to check antibacterial properties. Thereby, coatings of PHAG/PEM-5 showed a higher antibacterial activity and PHAG/PEM-4 a lower one, which was evidenced by plaque formation testing. Conclusively, PHAG/PEM coatings are promising for the reduction of implant-associated infections at surgical implants and thus may replace or complement established coatings based on low molecular synthetic antibiotics.

**KEYWORDS:** *bacteriophages, Staphylococcus aureus, polyelectrolyte multilayer, antibacterial properties, attenuated total reflection Fourier transform infrared spectroscopy, plaque assay*

## INTRODUCTION

Implant-associated infections pose a huge burden on health-care systems.[1,2] Traditionally, therapies based on systemic and local treatment with antibiotics are applied.[3] However, the development of resistance against common antibiotics will limit such classical treatments. Hence, alternative therapeutic approaches to conventional antibiotic-based ones are required. To overcome this problem and be independent from low molecular antibiotic-based compounds, alternative bactericide

Received: August 20, 2021
Accepted: November 12, 2021
Published: November 22, 2021







https://doi.org/10.1021/acsapm.1c01057
*ACS Appl. Polym. Mater.* 2021, 3, 6230−6237

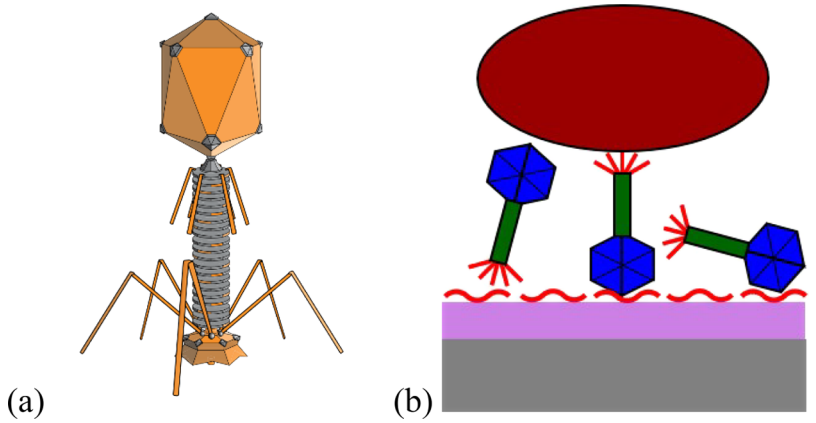


**Figure 1.** (a) Scheme of a typical bacteriophage (PHAG) with a head, collar, tube, plate, and feet (adapted from ref 6 with kind permission of M.D. Jones); (b) scheme of the antibacterial coating concept based on permanently bound PHAG at the outermost surface of predeposited polyelectrolyte (PEL) multilayers (PEM). PHAG adopt either a "tail-down−head-up", "head-down−tail-up", or "side-on" configuration (from left to right). Bacteria (brown) are bound and infected at immobilized PHAG.

concepts are developed. In that framework, the old concept of bacteriophages (PHAG) initiated by d'Hérelle,[4] which are expressed naturally by their host bacterial cells, has shown a renaissance. PHAG (Figure 1a) are ubiquitously occurring in the environment as the most abundant biological agent on earth.[5] PHAG are rodlike viruses composed of a head (capsid) storing either single- or double-stranded DNA and of a tail, through which the DNA is injected into host cells.

PHAG infect bacteria and therein replicate, transcript, and finally translate lytic peptide factors (e.g., endolysines). These lytic peptides destroy the host bacterium by defined binding and cleavage of the peptidoglycan-rich cell wall of, e.g., Gram-positive host bacteria. Due to the high osmotic pressure, the partly perforated host bacterium bursts by water influx. Hence, PHAG are increasingly used to replace common low molecular antibiotics in both home therapies of, e.g., respiratory diseases and are envisioned to treat complex bone and implant infections in orthopedic surgeries. While in certain countries (e.g., Canada and Georgia), PHAG-based home or clinical therapies are historically established, in the majority of countries, such therapies are still not approved officially, as there is still a massive lack of knowledge on their mechanism of action, dosage, and potential side effects.

Herein, innovative proteolytic coatings based on PHAG are introduced. Thereby, we like to combine this antibacterial concept with the classical one of surface premodification based on polyelectrolyte multilayers (PEM) deposited by the LbL concept initiated by Decher et al.[7] The LbL concept is based on the consecutive adsorption of selected polycations and polyanions from solution frequently starting with the polycation anchoring at the material of choice followed by the polyanion step and repeating this algorithm for desired times. This methodology has been frequently applied in the biomedical field for biopassivation, activation, and tissue engineering[8−15] and for membrane modification[16,17] all for different substrate geometries.

Concerning polyelectrolyte-mediated deposition of viruses and PHAG, Jabrane et al.[18] reported PHAG that were electrostatically bound at preadsorbed polycation monolayers. Other authors reported polyelectrolyte/virus assemblies and even polyelectrolyte/PHAG assemblies both deposited by the LbL concept, where viruses or PHAG are mainly integrated within the coating.[19,20] Less references prevail on alternating polycation/polyanion assemblies, where the virus is bound at the outermost layer of the assembly. Solely, Bacharouche et al.[21] reported various synthetic polycation/polyanion systems, whose outermost layer PHAG were bound and allowed to putatively "postdiffuse" into the given PEM system.

Following this concept, in this report, PHAG were specifically bound at predeposited PEM of poly(ethyleneimine) (PEI) and poly(acrylic acid) (PAA) on Ge model substrates using only few layers or adsorption steps. The PEI/PAA system was chosen since it has been well-established by us[22,23] and others[24] in the biomedical field. Either T4 PHAG or *Staphylococcus aureus* (S.a.) PHAG were utilized since they were well-established and available. Additionally, comparable specific and selective adsorption experiments have been performed by us using proteins[25,26] instead of PHAG. Herein, the influence of the outermost layer of PEM of PEI/PAA on PHAG binding was emphasized. In this framework, at first, the two- (PEI/PAA) and four-layer systems (PEI/PAA/PEI/PAA) as anionic PAA-terminating and the three- (PEI/PAA/PEI) and five-layer systems (PEI/PAA/PEI/PAA/PEI) as cationic PEI-terminating PEM systems were constructed. Afterward, the PEM-2, PEM-3, PEM-4, and PEM-5 systems were contacted with PHAG dispersions, and PHAG binding was studied by adsorption experiments. Finally, the biological activity of the S.a. PHAG-modified PEM at agar plates was investigated.

## EXPERIMENTAL PART

**Surface.** As model surfaces for the polyelectrolyte multilayer modification, plasma-cleaned (plasma chamber PDC-32G, Harrick (distributed by Starna, Pfungstadt), 1 Torr, 2 min, and 100 W) trapezoidal internal reflection elements (IRE) with dimensions of 50 mm × 20 mm × 2 mm of Ge ($n_1$ = 4.0, with dimensions 50 mm × 20 mm × 2 mm) were used.

**Polyelectrolyte Multilayers.** The polycation poly(ethyleneimine) (PEI, Aldrich, $M_w$ = 25.000 g/mol) and the polyanion poly(acrylic acid) (PAA, Sigma-Aldrich, $M_w$ = 50.000 g/mol) were used without further preparation. PEI and PAA were dissolved in deionized water (Millipore, 18.2 MΩ) to a concentration of 10 mmol/L resulting in values of pH = 10 and pH = 4 for PEI and PAA solutions, respectively. Polyelectrolyte multilayers (PEM) of PEI and PAA were fabricated by consecutive depositing/rinsing cycles above the Ge IRE in the sample compartment of the ATR-IR sorption cell (M.M., IPF Dresden) according to the stream coating procedure


https://doi.org/10.1021/acsapm.1c01057
ACS Appl. Polym. Mater. 2021, 3, 6230−6237

described in a study.[22] Between every PEL addition, the sorption cell was carefully rinsed with Millipore water.

**Bacteriophage Adsorption.** T4 bacteriophages (T4 PHAG, DSMZ, Braunschweig, Germany) and the *Staphylococcus aureus* bacteriophage (S.a. PHAG, Uniklinikum Regensburg, Germany) were used. Both original PHAG suspensions contained approximately a number of $10^{10}$ bacteriophages in 1 mL of buffered solutions (PBS and TRIS), which were diluted with Millipore water by a factor of 1:10 for the experiments reported herein. The PHAG binding measurements were performed directly at the freshly prepared PEM-coated Ge IRE in the ATR-IR sorption cell. A volume of 1 mL of the diluted PHAG suspension (1:10) was injected into the ATR-IR sorption cell and then contacted with the given PEM-coated Ge IRE for 30 min.

**Bacterial Testing.** To test the antibacterial activity of phages, either PEM-4 or PEM-5 of PEI/PAA were deposited onto own prepared standard Luria broth (LB) agar plates by consecutively pouring over them 2 mL of 0.01 M PEI, Millipore water, 0.01 M PAA, and Millipore water in this sequence. Thereafter, S.a. PHAG were adsorbed to either PEM-4- or PEM-5-modified agar plates. For this, 1 mL of diluted PHAG suspensions (1:100) was contacted with the given PEM for 30 min and then rinsed 3 times with Millipore water. Finally, plaque assay was performed on these pretreated agar plates, which were incubated for 24 h, and the formation of plaques was qualitatively followed by photography. Thereby, a bacterial strain of *S. aureus* EDCC 5055 was used. This strain was cultivated overnight in an LB medium. The next day, the overnight culture was subcultured into a fresh LB medium (1:100) and incubated on a shaker at 37 ° C, until it reached an optical density (OD) (UV/vis SmartSpec Plus spectrophotometer, Bio-Rad GmbH, Germany) of 1. A semisolid LB agar medium (0.7% agar) was liquefied by heating in a micro-oven. After cooling this medium to 45 °C, 4 mL of the bacterial culture was mixed with 30 mL of semisolid agar media. Each 5 mL of semisolid agar media was distributed onto the solid LB agar plates. After solidifying, the plates were incubated at 37 °C for the plaque formation. As a positive control, isolated S.a. PHAG ($10^9$) were used. For the negative control, sterile PBS was added. Constructs AGAR/PEM/PHAG (wet) were prepared in one lab (M.M.) and shipped to a partner lab (G.K.M.), and one week later, the bacterial tests were performed. Image analysis was performed using ImageJ software determining the area of clearance on the agar plates, and Sigma Plot was used for plotting and applying *t* tests for statistical analysis.

**Attenuated Total Reflection Infrared Fourier Transform (ATR-FTIR) Spectroscopy.** An in situ ATR-FTIR apparatus for sorption measurements[27] consisting of a special mirror setup (OptiSpec, Neerach, Switzerland) and an in situ sorption cell (M.M., IPF Dresden) was used on a commercial FTIR spectrometer (Vector 22, BRUKER-Optics GmbH, Ettlingen, Germany) equipped with a globar source and a mercury cadmium telluride (MCT) detector. ATR-FTIR absorbance spectra were recorded by the SBSR (single-beam sample reference) method, whereby single-channel spectra $I_{S,R}$ were recorded for both the upper (S) and lower (R) half of the Ge IRE (50 × 20 × 2 $mm^3$). Above the sample and reference half are two liquid chambers (S and R) sealed by O-rings (Viton), which were filled with polyelectrolyte or protein solution (S chamber) and with the solvent (R chamber), respectively. Ratioing the single-channel spectra according to $A_{SBSR} = -\log(I_S/I_R)$ resulted in absorbance spectra ($A_{SBSR}$) featuring proper compensation of the background absorptions due to the $GeO_xH_y$ layer, solvent (water and buffer), water vapor (spectrometer), and water condensate on the MCT detector window.

**Scanning Force Microscopy (SFM).** SFM was applied for the microscopic characterization of PHAG bound at the PEM surface. A Nanostation II (Bruker Nano GmbH, Berlin, Germany) including an optical microscope and an SFM component was used. For SFM, silicon probe tips from Nanosensors (Darmstadt, Germany) having apex radii of around 10 nm as cantilevers were utilized. PHAG bound at PEM films on Ge IRE were probed by noncontact mode (topography, error phase mode) operating with cantilevers at frequencies of around 160 kHz and free amplitudes of around 100 nm.

**Colloid Titration.** A particle charge detector (PCD-04 (Mütek), BTG, Eclepens, Switzerland) was used to determine the sign and amplitude of the PHAG net charge in PHAG suspensions ($10^{-9}$ PHAG per 1 mL) based on streaming potential measurements. At first, the PCD determined the amplitude and sign of the starting potential and thereupon dosed optionally the respective oppositely charged low molecular cationic 0.001 M poly-(diallyldimethylammonium chloride) (PDADMAC) or anionic 0.001 M sodium poly(ethylene-sulfonate) (PES) as titrator solutions into the diluted PHAG suspension sample. The consumed titrated volume of either 0.001 M PDADMAC (used herein) or 0.001 M PES solution (not used herein) needed for reaching a potential of zero was registered, from which the number or concentration of excess negatively (valid herein) or positively charged groups of PHAG can be determined.

## RESULTS AND DISCUSSION

**Polyelectrolyte Multilayer (PEM) Deposition.** At first, PEM were deposited by consecutive adsorption steps $z = 1$ up to 6 from PEI and PAA solutions at the Ge substrate, which was checked by in situ ATR-FTIR spectroscopy. In Figure 2a, a typical series of in situ ATR-FTIR spectra on PEM-6 deposition are shown.

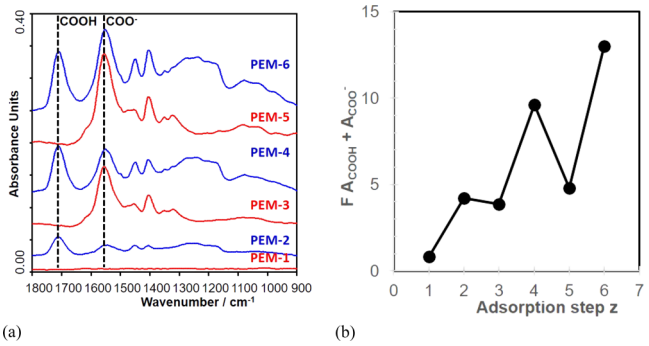


**Figure 2.** (a) In situ ATR-FTIR spectra of PEM films consecutively adsorbed from 0.01 M PEI and 0.01 M PAA solutions at the Ge substrate. PEM-1 refers to the film after the first PEI adsorption step (monolayer) and PEM-2 to PEM-6 to respective films after the second up to the sixth adsorption steps. (b) Summed integrals of $\nu$(C═O) and $\nu(COO^-)$ bands according to $F\,A_{COOH} + A_{COO^-}$ as a measure for the PEM (PAA) deposited amount. A factor $F = 2$ was used to take the different absorption coefficients of the two IR bands into account.

The diagnostic $\nu$(C═O) band at around 1705 $cm^{-1}$ and the $\nu_{as}(COO^-)$ band at around 1550 $cm^{-1}$ due to respective carboxyl (COOH) and carboxylate ($COO^-$) groups of the bound PAA were used for quantification of the deposited PEM amount. In Figure 2b, the sum of the respective band integrals $F\,A_{COOH} + A_{COO^-}$ is plotted versus the adsorption step *z*, from which PEM deposition can be monitored quantitatively as published earlier.[22] Evidently, a rather nonlinearly increasing course was obtained, which we commented on recently.[28] Briefly, upon deposition of PEI layers, the Ge surface gets positively overcharged and upon deposition of PAA layers gets negatively overcharged. The bound amount of PAA increases in the even (PAA) adsorption steps (PEM-2, PEM-4, and PEM-6), while in the odd (PEI) steps (PEM-3 and PEM-5), it decreases with respect to the latter even step. This observation has been attributed to a part rupture or pull-out of the last adsorbed PAA in the step $z = N$ by the present oppositely


https://doi.org/10.1021/acsapm.1c01057
ACS Appl. Polym. Mater. 2021, 3, 6230−6237

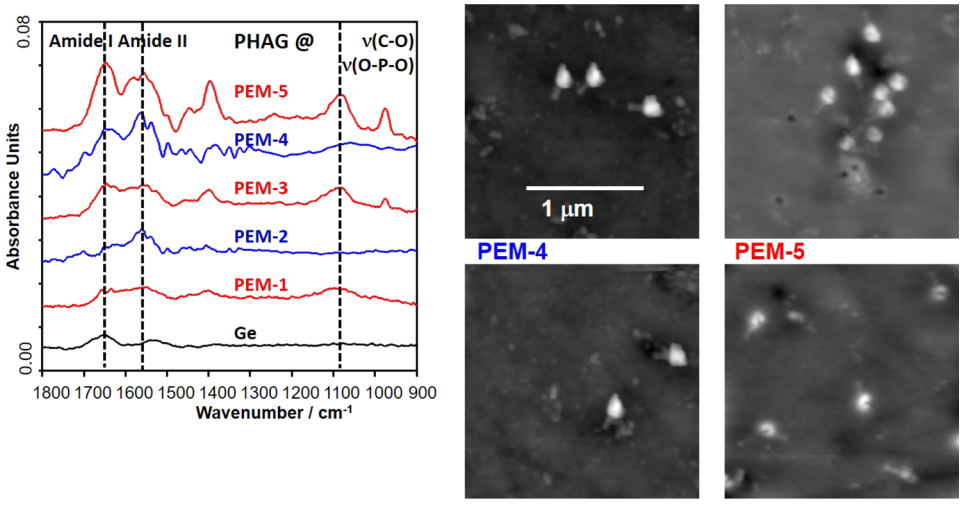


**Figure 3.** (a) ATR-FTIR difference spectra on bound PHAG (T4) at PEM-1, PEM-2, PEM-3, PEM-4, and PEM-5 deposited at Ge substrates. Broken vertical lines indicate diagnostic bands (Amide I, Amide II, $\nu$(C−O), and $\nu$(O−P−O), see the text). (b) Representative SFM images (topography) of T4 PHAG bound to either PEM-4 (left, top and bottom) or PEM-5 (right, top and bottom) at Ge substrates corresponding to the respective ATR-FTIR spectra in Figure 2 (image scale: 2 × 2 $\mu$m).

charged PEI in the subsequent step $z = N + 1$, which has been also observed for other oppositely charged PEL pairs.[29] A rather strong increase in the bound PAA amount could be identified, which has been attributed to strong acid/base interactions between PEI and PAA under the chosen pH conditions (PEI, pH = 10; PAA, pH = 4) reported earlier.[28] Hence, the PEI/PAA system allows a sustained surface modification of a wide range of model and applied substrate materials including planar, curved, or porous geometries and bearing both charged and uncharged surface functionalities, utilizing only a small number of adsorption steps and low amounts of PEL materials. To characterize the charge properties of PEI/PAA coatings further, electrokinetic measurements on either PEI- or PAA-terminated PEM at glass substrates were performed. Exemplary results are given in Figure S4 of the Supporting Information. Therein, zeta potential versus pH profiles significantly show a cationic surface charge for PEI-terminated and an anionic surface charge for PAA-terminated PEM. Furthermore, contact angle measurements were performed at PEM-5 and PEM-6 of PEI/PAA multilayers at glass substrates. For both systems PEM-5 and PEM-6, the contact angles were dynamically unstable and decreased during the measurements within 1−2 min, presumably due to surface heterogeneity and roughness. While for PEM-5, contact angles underwent large decreases starting from around 90 down to 50°, smaller decreases starting from around 50 down to 25° were obtained for PEM-6. Hence, qualitatively, the surface of PEM-6 appeared more hydrophilic than PEM-5. Since obviously, PEM coatings of PEI/PAA provide a polymer platform exposing either a cationic or anionic surface charge, charged biological compounds can be either bound or rejected in the sense of bioactivation or biopassivation. In the following section, this is utilized for the immobilization of PHAG.

**Bacteriophage (PHAG) Binding at PEM.** Consequently, PHAG were bound on PEM of PEI/PAA under variation of the used adsorption step $z$ (i.e., layer number), thus exposing different surface charges due to either PEI or PAA as the terminating layer. In situ ATR-FTIR spectroscopy was used as the analytical tool. Both T4 PHAG and *Staphylococcus aureus* (S.a.) PHAG were used.

*T4 PHAG.* In Figure 3a, ATR-FTIR difference spectra between PEM, to which PHAG dispersions were contacted (PHAG@PEM), and pure PEM are shown for PEM-1 up to PEM-5.

From the spectra of the given PEM after contact with the PHAG dispersion for 1 h, the respective spectra before contact were subtracted. Such difference spectra correspond to the bound PHAG amount at these PEM systems. Generally, in these difference spectra, contributions of not fully compensated absorptions of the PEM material occurred, and absorptions from PHAG were rather low. Nevertheless, at 1090 $cm^{-1}$ (vertical broken line in Figure 3a), a pronounced band was obtained in all PEI-terminated PEM, which could be attributed to either phosphate moieties ($\nu$(O═P═O) vibration) of packed DNA or to saccharide hydroxyls or linkages ($\nu$(C−O) vibration) of glycoproteins diagnostic of PHAG. Likewise, signals in the Amide I and Amide II band regions between 1700 and 1500 $cm^{-1}$, which can be assigned to amide groups of such glycoproteins, are visible in the difference spectra of PEI-terminated PEM (PEM-1, PEM-3, and PEM-5). Significantly, these diagnostic IR band absorptions were lower in the difference spectra of PAA-terminated PEM (PEM-2 and PEM-4), indicating a lower PHAG bound amount. Presumably, the higher binding of PHAG at the cationic outermost layer PEI could be due to attractive electrostatic interaction with anionic glycoproteins of the capsid around the PHAG head or tail. Such attractive interactions between anionic glycoproteins of the capsid and the outermost PEI layer of PEM have been reported earlier also for other anionic model proteins on a quantitative level.[25,26] In contrast, such anionic capsidic glycoproteins of PHAG are supposed to be responsible for the observed lower binding at PEM-2 and PEM-4 terminated by like charged PAA. Of course, the packed DNA in the PHAG head as a natural highly charged polyanion may be also addressed for such electrostatic attraction or repulsion at respective PEI- or PAA-terminated PEM. However, the PHAG capsid layer and the


https://doi.org/10.1021/acsapm.1c01057
ACS Appl. Polym. Mater. 2021, 3, 6230−6237

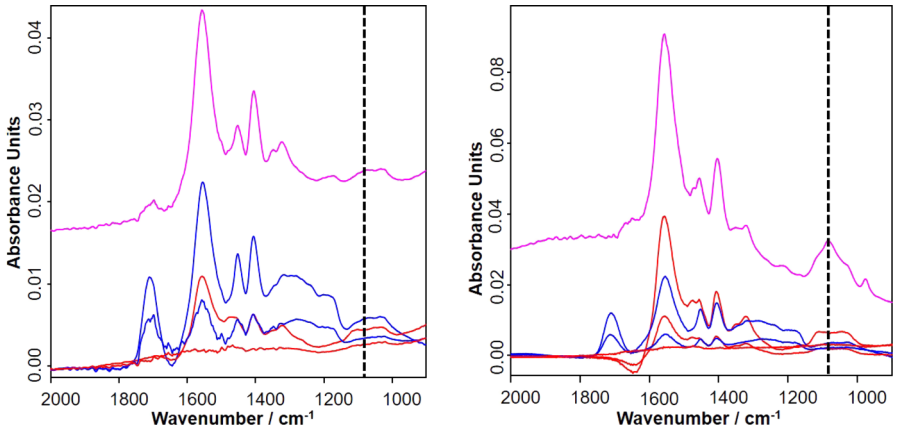


**Figure 4.** (a) In situ ATR-FTIR spectra of PEM-1, PEM-2 (blue), PEM-3 (red), and PEM-4 (blue) and of PEM-4, at which S.a. PHAG were bound (pink). (b) In situ ATR-FTIR spectra of PEM-1 (red), PEM-2 (blue), PEM-3 (red), PEM-4 (blue), and PEM-5 (blue) and of PEM-5, at which S.a. PHAG were bound (pink).

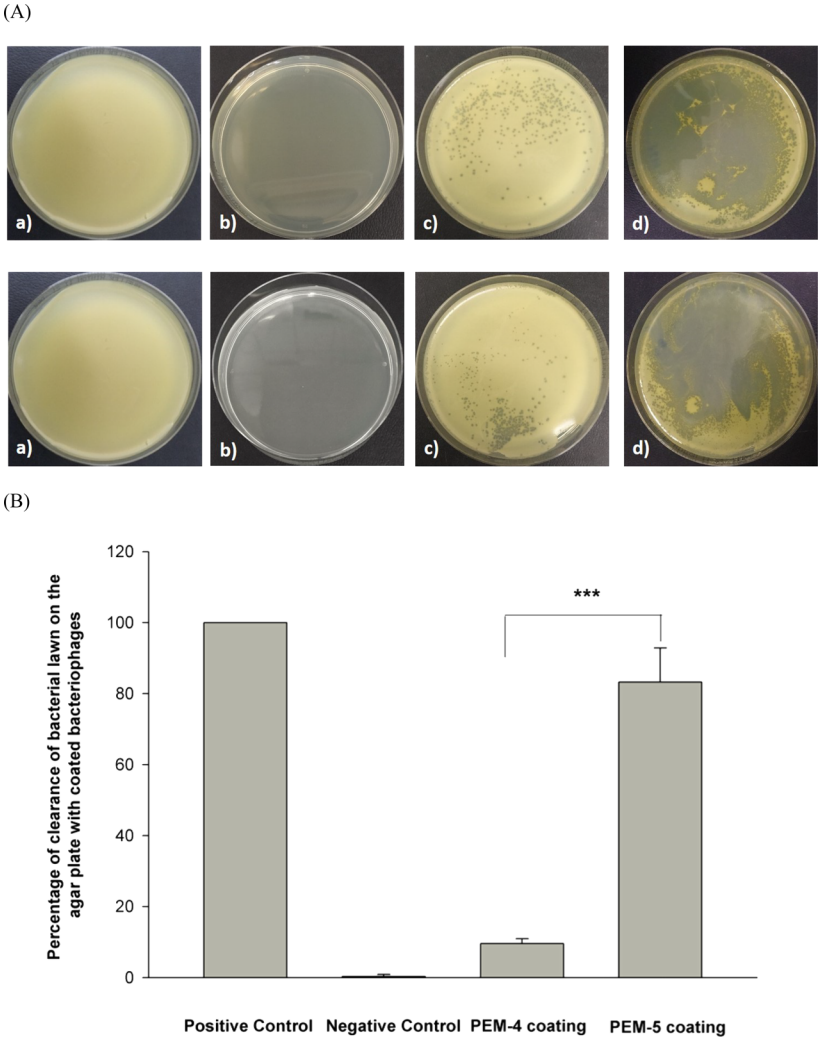


**Figure 5.** (A) Antibacterial activity of S.a. PHAG adsorbed either to PEM-4 or PEM-5 on LB agar plates. (a) Negative control with pure PBS buffer and an *S. aureus* bacterial suspension in semisolid agar onto LB agar plates without PHAG, (b) positive control with $10^9$ PHAG and *S. aureus* on LB agar, (c) LB agar plate with PHAG adsorbed on PEM-4 and plaque assay with *S. aureus*, and (d) LB agar plate with PHAG on PEM-5 and plaque assay with *S. aureus*. Two representative runs for PEM-4 (c) and PEM-5 (d) are shown on the first and second row, respectively. (B) Bar plot on the antibacterial activity of PEM-4 and PEM-5 based on the analysis of images exemplarily given in (A).



https://doi.org/10.1021/acsapm.1c01057
ACS Appl. Polym. Mater. 2021, 3, 6230−6237

high ionic strength in the PHAG head are assumed to shield or reduce the electrostatic reach of the DNA charge significantly.

*Microscopy.* Corresponding to these ATR-FTIR spectra, SFM images on bound T4 PHAG at PEM-4 and PEM-5 of PEI/PAA are given in Figure 3b. Two representative images are shown for PHAG at PEM-4 (left) and PEM-5 (right). Evidently, in all images, single PHAG can be identified in the images with the characteristic nanostructure consisting of a thick head and a thin tail. More details show exemplary SFM profiles of the head width, tail width, and total length of exemplary single PHAG at PEM-4 and PEM-5, which are given in Figure S2 of the Supporting Information. Therein, for T4 PHAG at PEM-4, total lengths of around 200−250 nm with a head/tail ratio of around 1.5 can be found. Individual feet at the end of the tail could not be detected due to the insufficient resolution of the SFM image. Interestingly, for PHAG at PEM-4, the height values of the head (≈30 nm) and the tail (≈8 nm) were significantly higher compared to those of the head (≈14 nm) and the tail (≈3 nm) for PEM-5. Obviously, PHAG at PEM-5 appear qualitatively to be more "sinked in" and integrated in the PEM phase compared to PEM-4 presumably due to stronger electrostatic attraction.

Moreover, only 2−3 T4 PHAG could be found in the respective representative images for PEM-4, while 7−8 T4 PHAG show up in the respective representative images for PEM-5. Being aware of the rather poor statistics, we observed that obviously less T4 PHAG were bound at PEM-4 exposing a negative excess surface charge due to PAA, while more T4 PHAG were bound at PEM-5 exposing a cationic excess surface charge due to PEI. Hence, the number of T4 PHAG in the images corresponds qualitatively to the intensity of the IR band at 1090 $cm^{-1}$ diagnostic of PHAG, which supports the ATR-FTIR results.

*S.a. PHAG.* In addition to the interaction of T4 PHAG to PEM, also that of S.a. PHAG was studied. In Figure 4a, ATR-FTIR spectra of PEM-1 to PEM-4 and of PEM-4 to which an S.a. PHAG dispersion was brought into contact are shown.

Likewise, in Figure 4b, ATR-FTIR spectra of PEM-1 to PEM-5 and of PEM-5 brought into contact with PHAG are shown. While from Figure 4a, a rather low S.a. PHAG binding at PEM-4 could be obtained (broken vertical line for the diagnostic $\nu$(C−O) or $\nu$(O−P−O) band), S.a. PHAG binding at PEM-5 was rather high (corresponding vertical broken line), which in principle confirms the electrostatic binding modalities of T4 PHAG. Obviously, S.a. PHAG also bind stronger at the PEM surface terminated by PEI, which has a cationic excess charge compared to PEM terminated by PAA bearing an anionic excess charge. Again, anionic capsid proteins are suggested to be responsible for this charge-specific binding at PEI-terminated cationic PEM or respective repulsion at PAA-terminated anionic PEM. To check the anionic nature of S.a. PHAG further, colloid titration measurements were performed on suspensions of S.a. PHAG diluted by a factor of 1:10 resulting in concentrations of $10^{-9}$ PHAG per mL. Indeed, by colloid titration, a negative starting potential was observed, and consequently, the PHAG suspension was titrated by a standard 0.001 M low molecular cationic poly-(diallyldimethylammonium chloride) (PDADMAC) solution to a potential of zero, which confirms qualitatively the anionic nature of PHAG. Around 0.25 mL of 0.001 M PDADMAC solution was consumed, from which the number of excess negatively charged groups within PHAG can be calculated, which will be reported elsewhere.

**Bacterial Testing of PEM-Bound PHAG.** In Figure 5A,B, results of S.a. PHAG antibacterial tests on agar plates, which have been directly modified with either PEM-4 or PEM-5 and onto which S.a. PHAG were adsorbed, are presented.

In principle, the formation of plaques (plaque forming units (PFU)) describing the bacterial clearance or eradication was followed for control and modified agar plates after culturing *S. aureus* bacteria for 24 h. Obviously, nearly no plaque formation was found for pure agar (positive control) and complete plaque formation (clearance) for agar directly treated with PHAG (negative control). For the PEM (PEI/PAA)-modified agar plate, at which PHAG were adsorbed, lower plaque formation at around 10% of the agar plate was obtained for PEM-4, while a higher clearance of around 85% was observed for PEM-5. This indicates effective clearance of the bacteria by PHAG/PEM-5 and a less effective one by PHAG/PEM-4, which can be explained by the higher adsorbed amount of PHAG at positively charged PEM-5 due to electrostatic attraction of PHAG compared to the lower bound PHAG amount at negatively charged PEM-4, as it was shown above.

Actually, it is challenging to explain how surface-immobilized (i.e., confined) PHAG are able to contact with bacteria and form plaques and subsequently form bacterial clear zones that significantly. First of all, we like to emphasize that the best experimental efforts have been performed to wash out any loosely bound PHAG from the AGAR/PEM/PHAG constructs by exhaustive rinsing. Consequently, we assume that the remaining PHAG are well-bound at the outermost PEM. Furthermore, premixing the bacteria with semisolid agar media and pouring onto the AGAR/PEM/PHAG constructs result in AGAR/PEM/PHAG/bacterium constructs (interaction zones), where the bacteria are assumed to be in direct contact with the outermost bound PHAG. Some of those might be in the head-down−tail-up configuration (Figure 1b) allowing infection. Consequently, based on recent studies,[30−33] the PHAG are assumed to specifically interact with bacteria through a receptor and subsequently release their DNA inside the bacteria, whereafter DNA replication and transcription machinery starts, producing new PHAG particles. Thereafter, these multiplied PHAG particles are released upon cell wall lysis and burst of the bacteria. Simultaneously, lytic peptides might also be released upon bacterial damage allowing them to act on other bacteria. However, they might be not so effective to lyse other bacteria as their concentration is less. Finally, after bacterial lysis, the released PHAG can again lyse other surrounding bacteria, which eventually leads to the plaque and clear zone formation and thus bacterial reduction as evident in Figure 5Ad.

## CONCLUSIONS

Based on earlier studies on protein adsorption at polyelectrolyte multilayers (PEM),[25,26] we present herein in situ ATR-FTIR spectroscopic data on PHAG adsorption at the two-, three-, four-, five-, and six-layer (PEM-2, PEM-3, PEM-4, PEM-5, and PEM-6) systems of poly(ethyleneimine) (PEI) alternating with poly(acrylic acid) (PAA). Both T4 and S.a. model PHAG were used. PEM could be deposited reproducibly, providing well-defined model platforms for studying charge-driven PHAG binding addressing biomedical applications. Generally, the influence of the outermost layer and thus the outermost surface charge sign of PEM on PHAG adsorption was studied. Significantly lower PHAG adsorbed amounts were found at even numbered PEM terminated with



https://doi.org/10.1021/acsapm.1c01057
ACS Appl. Polym. Mater. 2021, 3, 6230−6237

anionic PAA, while higher PHAG adsorbed amounts were obtained at odd numbered PEM terminated with cationic PEI. This result suggests electrostatic interaction of PHAG with PEM for both T4 and S.a. PHAG types presumably based on the anionic nature of the capsid proteins enveloping the PHAG head or tail. Furthermore, agar plates, which have been modified by either PEM-4 or PEM-5, at which S.a. PHAG were bound in different respective amounts, showed different antibacterial activities. While at PEM-4 featuring a lower bound PHAG amount, a lower antibacterial activity was found, at PEM-5 featuring a higher bound PHAG amount, a higher antibacterial activity was observed. Trying to contribute to the challenging mechanism, we suggest anchoring of bacteria at the peripherally bound PHAG of PEM followed by DNA injection, replication, and proliferation of new PHAG. Afterward, bacterial burst releases both newly formed PHAG as well as lytic peptides attacking further bacteria in the bulk phase in an amplification scenario. Conclusively, these results show a straightforward concept to bind therapeutic PHAG at material surfaces via PEM predeposition followed by PHAG post-deposition contributing to novel antibacterial concepts not based on low molecular antibiotics, which is important to overcome the multiresistance dilemma toward bacteria.

## ■ ASSOCIATED CONTENT

### Supporting Information

The Supporting Information is available free of charge at https://pubs.acs.org/doi/10.1021/acsapm.1c01057.

Additional scanning force microscopy (SFM) data on PEI/PAA multilayers without and with PHAG and contact angle and zeta potential data on PEI/PAA multilayers on glass slides (PDF)

## ■ AUTHOR INFORMATION


### Corresponding Author

**Martin Müller** − *Department Functional Colloidal Materials, Leibniz-Institut für Polymerforschung Dresden e.V., Dresden 01069, Germany; Chair of Macromolecular Chemistry, Technische Universität Dresden, Dresden 01062, Germany;* orcid.org/0000-0001-8961-4604; Email: mamuller@ipfdd.de

### Authors

**Birgit Urban** − *Department Functional Colloidal Materials, Leibniz-Institut für Polymerforschung Dresden e.V., Dresden 01069, Germany*

**Gopala Krishna Mannala** − *Department of Trauma Surgery, Universitätsklinikum Regensburg, Regensburg 93053, Germany*

**Volker Alt** − *Department of Trauma Surgery, Universitätsklinikum Regensburg, Regensburg 93053, Germany*

Complete contact information is available at: https://pubs.acs.org/10.1021/acsapm.1c01057


### Notes

The authors declare no competing financial interest.

## ■ ACKNOWLEDGMENTS

This work is related to a recently submitted DFG proposal. Marina Oelmann and Gudrun Petzold (IPF) are thanked for the skillful contact angle and zeta potential measurements. Michael Dave Jones is thanked for allowing to use his artwork (Wikipedia) in Figure 1a.

## ■ REFERENCES


(1) Gristina, A. G.; Naylor, P.; Myrvik, Q. Infections from biomaterials and implants − a race for the surface. *Med. Prog. Technol.* **1989**, *14*, 205−224.

(2) Kildow, B. J.; Della-Valle, C. J.; Springer, B. D. Single vs 2-stage revision for the treatment of periprosthetic joint infection. *J. Arthroplasty* **2020**, *35*, 24−30.

(3) Alt, V. Antimicrobial coated implants in trauma and orthopedics - A clinical review and risk-benefit analysis. *Injury* **2017**, *48*, 599−607.

(4) d'Hérelle, F. Sur un microbe invisible antagoniste des bacilles dysentérique. *Acta Kravsi* **1917**, *165*, 373−375.

(5) Wommack, K. E.; Colwell, R. R. Virioplankton: Viruses in aquatic ecosystems. *Microbiol. Mol. Biol. Rev.* **2000**, *64*, 69−114.

(6) https://upload.wikimedia.org/wikipedia/commons/thumb/4/4a/PhageExterior.svg/800px-phageExterior.svg.png.

(7) Decher, G.; Hong, J. D.; Schmitt, J. Buildup of ultrathin multilayer films by a self-assembly process: III. Consecutively alternating adsorption of anionic and cationic polyelectrolytes on charged surfaces. *Thin Solid Films* **1992**, *210-211*, 831−835.

(8) Reyes, D. R.; Perruccio, E. M.; Becerra, S. P.; Locascio, L. E.; Gaitan, M. Micropatterning neuronal cells on polyelectrolyte multilayers. *Langmuir* **2004**, *20*, 8805−8811.

(9) Tang, Z.; Wang, Y.; Podsiadlo, P.; Kotov, N. A. Biomedical applications of layer-by-layer assembly: From biomimetics to tissue engineering. *Adv. Mater.* **2006**, *18*, 3203−3224.

(10) De Geest, B. G.; De Koker, S.; Sukhorukov, G. B.; Kreft, O.; Parak, W. J.; Skirtach, A. G.; Demeester, J.; De Smedt, S. C.; Hennink, W. E. Polyelectrolyte microcapsules for biomedical applications. *Soft Matter* **2009**, *5*, 282−291.

(11) Boudou, T.; Crouzier, T.; Ren, K.; Blin, G.; Picart, C. Multiple functionalities of polyelectrolyte multilayer films: New biomedical applications. *Adv. Mater.* **2010**, *22*, 441−467.

(12) Costa, R. R.; Mano, J. F. Polyelectrolyte multilayered assemblies in biomedical technologies. *Chem. Soc. Rev.* **2014**, *43*, 3453−3479.

(13) Olenych, S. G.; Moussallem, M. D.; Salloum, D. S.; Schlenoff, J. B.; Keller, T. C. S. Fibronectin and cell attachment to cell and protein resistant polyelectrolyte surfaces. *Biomacromolecules* **2005**, *6*, 3252−3258.

(14) Shah, N. J.; Macdonald, M. L.; Beben, Y. M.; Padera, R. F.; Samuel, R. E.; Hammond, P. T. Tunable dual growth factor delivery from polyelectrolyte multilayer films. *Biomaterials* **2011**, *32*, 6183−6193.

(15) Lichter, J. A.; Van Vliet, K. J.; Rubner, M. F. Design of antibacterial surfaces and interfaces: Polyelectrolyte multilayers as a multifunctional platform. *Macromolecules* **2009**, *42*, 8573−8586.

(16) Stanton, B. W.; Harris, J. J.; Miller, M. D.; Bruening, M. L. Ultrathin, multilayered polyelectrolyte films as nanofiltration membranes. *Langmuir* **2003**, *19*, 7038−7042.

(17) Abtahi, S. M.; Ilyas, S.; Cassan, C. J.; Albasi, C.; de Vos, W. M. Micropollutants removal from secondary-treated municipal wastewater using weak polyelectrolyte multilayer based nanofiltration membranes. *J. Membr. Sci.* **2018**, *548*, 654−666.

(18) Jabrane, T.; Dubé, M.; Mangin, P. J. Bacteriophage immobilization on paper surface: Effect of cationic pre-coat layer. *Proceedings of Pulp and Paper Technical Association Canada* **2009**, *95*, 311−315. (PAPTAC 95th Annual Meeting)

(19) Lin, Y.; Su, Z.; Niu, Z.; Li, S.; Kaur, G.; Lee, L. A.; Wang, Q. Layer-by-layer assembly of viral capsid for cell adhesion. *Acta Biomater.* **2008**, *4*, 838−843.

(20) Dorval Courchesne, N. M.; Klug, M. T.; Chen, P. Y.; Kooi, S. E.; Yun, D. S.; Hong, N.; Fang, N. X.; Belcher, A. M.; Hammond, P. T. Assembly of a bacteriophage-based template for the organization of materials into nanoporous networks. *Adv. Mater.* **2014**, *26*, 3398−3404.

(21) Bacharouche, J.; Erdemli, O.; Rivet, R.; Doucouré, B.; Caillet, C.; Mutschler, A.; Lavalle, P.; Duval, J. F. L.; Gantzer, C.; Francius, G. On the infectivity of bacteriophages in polyelectrolyte multilayer films: Inhibition or preservation of their bacteriolytic activity? *ACS Appl. Mater. Interfaces* **2018**, *10*, 33545−33555.
(22) Müller, M.; Rieser, T.; Lunkwitz, K.; Berwald, S.; Meier-Haack, J.; Jehnichen, D. An in-situ ATR-FTIR study on polyelectrolyte multilayer assemblies on solid surfaces and their susceptibility to fouling. *Macromol. Rapid Commun.* **1998**, *19*, 333−336.
(23) Müller, M.; Rieser, T.; Lunkwitz, K.; Meier-Haack, J. Polyelectrolyte complex layers: a promising concept for antifouling coatings verified by in-situ ATR-FTIR spectroscopy. *Macromol. Rapid Commun.* **1999**, *20*, 607−611.
(24) Deng, Y.; Sun, J.; Ni, X.; Xiong, D. Multilayers of poly(ethyleneimine)/poly(acrylic acid) coatings on Ti6Al4V acting as lubricated polymer-bearing interface. *J. Biomed. Mater. Res.* **2020**, *108B*, 2141−2152.
(25) Müller, M.; Rieser, T.; Dubin, P. L.; Lunkwitz, K. Selective interaction between proteins and the outermost surface of polyelectrolyte multilayers: Influence of the polyanion type, pH and salt. *Macromol. Rapid Commun.* **2001**, *22*, 390−395.
(26) Müller, M.; Keßler, B.; Houbenov, N. pH dependence and protein selectivity of poly(ethyleneimine)/poly(acrylic acid) multilayers studied by in situ ATR-FTIR spectroscopy. *Biomacromolecules* **2006**, *7*, 1285−1294.
(27) Fringeli, U. P. '*Encyclopedia of Spectroscopy and Spectrometry*', Lindon, J. C.; Tranter, G. E.; Holmes, J. L. Eds., Academic Press, N. Y. (2000)
(28) Müller, M. The anomalous influence of polyelectrolyte concentration on the deposition and nanostructure of poly(ethyleneimine)/poly(acrylic acid) multilayers. *Molecules* **2019**, *24*, 2141.
(29) Müller, M.; Urban, B.; Schwarz, S. Biorelated polyelectrolyte coatings studied by in-situ attenuated total reflection-Fourier transform infrared spectroscopy: Deposition concepts, wet adhesiveness and biomedical applications. *Langmuir* **2018**, *34*, 8129−8144.
(30) Love, M. J.; Bhandari, D.; Dobson, R. C. J.; Billington, C. Potential for bacteriophage endolysins to supplement or replace antibiotics in food production and clinical care. *Antibiotics* **2018**, *7*, 17.
(31) Schuch, R.; Khan, B. K.; Raz, A.; Rotolo, J. A.; Wittekind, M. Bacteriophage lysin CF-301, a potent antistaphylococcal biofilm agent. *Antimicrob. Agents Chemother.* **2017**, *61*, No. e02666-16.
(32) Schmelcher, M.; Donovan, D. M.; Loessner, M. J. Bacteriophage endolysins as novel antimicrobials. *Future Microbiol.* **2012**, *7*, 1147−1171.
(33) Abdelrahman, F.; Easwaran, M.; Daramola, O. I.; Ragab, S.; Lynch, S.; Oduselu, T. J.; Khan, F. M.; Ayobami, A.; Adnan, F.; Torrents, E.; Sanmukh, S.; El-Shibiny, A. Phage-encoded endolysins. *Antibiotics* **2021**, *10*, 124.





https://doi.org/10.1021/acsapm.1c01057
*ACS Appl. Polym. Mater.* 2021, 3, 6230−6237